

Synthesizing the Transmission Properties of a Five-Bar Linkage by Shaping Workspace Bounds

Shashank Ramesh and Mark Plecnik^(⊠)

University of Notre Dame, Notre Dame, IN 46556, USA {sramesh,plecnikmark}@nd.edu

Abstract. The multidirectional transmission characteristics of a fivebar linkage can be visualized by plotting Jacobian-defined velocity ellipses inside its workspace. The orientation, size, and aspect ratio of these ellipses indicate directional force and velocity multiplication from the actuators to the end-effector. Our broader goal is approximate dimensional synthesis to achieve desired ellipses. On a workspace bound, the minor axis of a velocity ellipse collapses while the major axis aligns tangential to the bound. Interior to the workspace, ellipses vary with continuity. Therefore, the shape of a workspace bound influences the interior ellipses. The workspace bounds of a five-bar linkage are formed from segments of four-bar coupler curves (the locus of endpoint positions while the five-bar is held in output singularity conditions) and circular segments. Therefore, interior ellipses can be influenced by the path synthesis of four-bar linkages that represent the five-bar situated with certain links held colinear (the output singularity conditions). This paper details the synthesis of these four-bar coupler curves for forming the workspace bounds of a five-bar in order to influence its interior ellipses. Our approach employs saddle graphs that detail the connectivity of critical points over an optimization function.

1 Introduction

The velocity and force transmission characteristics of a parallel mechanism is determined by the first-order kinematics. A well-known visualization of the force/velocity transmission characteristics is the *velocity ellipse* as described by the Jacobian matrix that encodes the first-order kinematics of the mechanism. Inside the workspace of a mechanism, the desired force/velocity transmission characteristics can be achieved by appropriately orienting and sizing the velocity ellipses. For example, high vertical forces at the end-effector of a mechanism can be produced for low actuator torques by orienting the minor axes of the velocity ellipses vertically in the desired portion of the workspace. Such mechanisms may find utility as legs of robots and industrial manipulators that need to carry heavy vertical loads for pick-and-place operations. In this work, we propose the concept of shaping workspace boundaries to influence the orientation,

size, and aspect ratio of the velocity ellipses inside the workspace. This concept is demonstrated in this manuscript by considering a five-bar mechanism. At a workspace boundary, the velocity ellipse has zero minor axis length and its major axis is tangential to the workspace boundary. Thus, given the continuous kinematics of the mechanism, the orientation of a velocity ellipse close to a workspace boundary is heavily influenced by the local shape of the workspace boundary. This forms the main motivation for this work.

In literature, several works can be found on designing five-bar mechanisms for path generation and workspace for optimal performance in terms of force transmission, dexterity, etc. Methods for path generation using geared five-bars have been presented in [1,2]. Five-bar design methodologies for improving energy efficiency over specific trajectories or regions inside the workspace have been proposed in [3,4]. The design methodology in [5] aims to maximize the dexterous workspace of the five-bar by eliminating singularities inside the workspace. In [6], the optimal design of the five-bar is carried out by studying performance indices based on end-effector velocity and force production. However, these methods do not explicitly synthesize velocity ellipses to achieve the desired bias in force/velocity transmission. In this regard, Plecnik in [7] details a method to synthesize five-bar mechanisms that exactly produce two given velocity ellipses. In contrast, this work aims to approximately orient and size many velocity ellipses inside the workspace by appropriately shaping the workspace boundaries. The synthesis approach makes use of saddle graphs [8], in order to explore the connections between critical points across an optimization function. In the following, the kinematics of the five-bar mechanism are discussed in Sect. 2. The problem of shaping workspace boundaries for a five-bar mechanism is formulated in Sect. 3, and a solution method is detailed in Sect. 4. A numerical example is presented in Sect. 5, and Sect. 6 concludes the work.

2 Kinematics of the Five-Bar Mechanism

Figure 1(a) shows the kinematic diagram of a five-bar mechanism displaced from a known reference configuration given by: \mathbf{A}_0 , \mathbf{B}_0 , \mathbf{C}_0 , \mathbf{D}_0 , \mathbf{F}_0 , \mathbf{P}_0 . A global frame $\{1\}$ is defined with its origin at \mathbf{O} . The actuators situated at \mathbf{A}_0 and \mathbf{B}_0 are fixed to ground and displace the links $\mathbf{A}_0\mathbf{C}$ and $\mathbf{B}_0\mathbf{D}$ by angles ϕ and ψ , respectively. The kinematic constraints relating the input variables $\mathbf{\theta} = [\phi \ \psi]^{\top}$ and the output variables $\mathbf{P} = [x \ y]^{\top}$ are given by:

$$\mathbf{A}_{0} + [\mathcal{R}(\phi)] (\mathbf{C}_{0} - \mathbf{A}_{0}) + [\mathcal{R}(\rho)] (\mathbf{F}_{0} - \mathbf{C}_{0})$$

$$= \mathbf{B}_{0} + [\mathcal{R}(\psi)] (\mathbf{D}_{0} - \mathbf{B}_{0}) + [\mathcal{R}(\theta)] (\mathbf{F}_{0} - \mathbf{D}_{0}),$$
(1)

$$\mathbf{A}_0 + \left[\mathcal{R}(\phi) \right] (\mathbf{C}_0 - \mathbf{A}_0) + \left[\mathcal{R}(\rho) \right] (\mathbf{P}_0 - \mathbf{C}_0) = \mathbf{P}. \tag{2}$$

In Eqs. (1, 2), ρ and θ are known as intermediate variables. They describe passive link orientations that belong to neither the input nor output space. Introduce the notation \mathbf{r}_{ij} , $i, j \in \{A, B, C, D, F, P\}$, that is the vector from the pivot i to

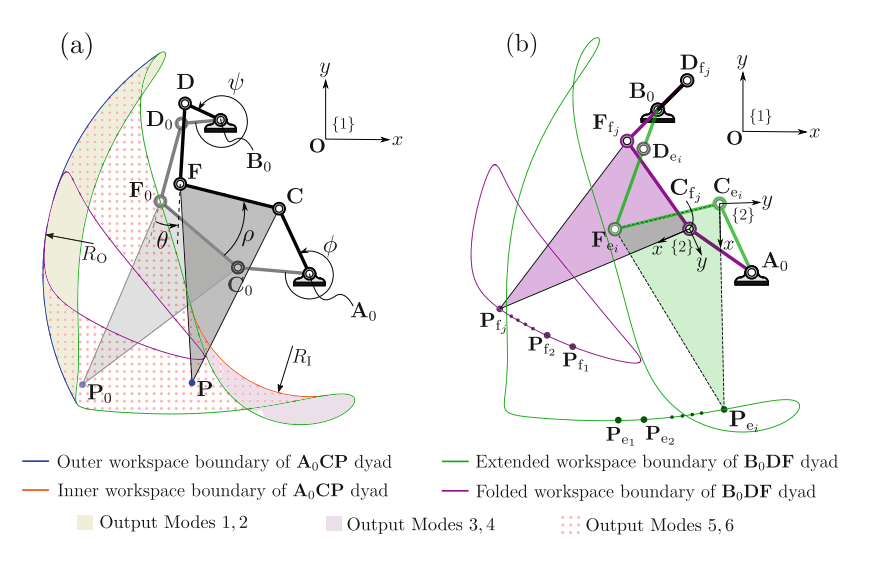


Fig. 1. (a) Kinematic diagram of a five-bar mechanism, (b) Four-bars arising from the alignment of the links of $\mathbf{B}_0\mathbf{DF}$ dyad whose coupler curves are the workspace boundaries of the five-bar in (a).

pivot j, e.g., $\mathbf{r}_{DF}(\theta) = [\mathcal{R}(\theta)] (\mathbf{F}_0 - \mathbf{D}_0)$. Differentiating Eqs. (1, 2) and eliminating $\dot{\rho}$, $\dot{\theta}$, the Jacobian matrix [J] takes the form,

$$[J] = \left[\mathbf{J}_{1} \ \mathbf{J}_{2} \right], \quad \text{where,}$$

$$\mathbf{J}_{1} = \left[i \ \right] \left(\mathbf{r}_{AC}(\phi) - \frac{\mathbf{r}_{DF}(\theta) \times \mathbf{r}_{AC}(\phi)}{\mathbf{r}_{DF}(\theta) \times \mathbf{r}_{CF}(\rho)} \mathbf{r}_{CP}(\rho) \right),$$

$$\mathbf{J}_{2} = \frac{\mathbf{r}_{DF}(\theta) \times \mathbf{r}_{BD}(\phi)}{\mathbf{r}_{DF}(\theta) \times \mathbf{r}_{CF}(\rho)} \left[i \ \right] \mathbf{r}_{CP}.$$

$$(3)$$

The symbol "×" above denotes the 2D analog of the cross product, i.e. $\mathbf{a} \times \mathbf{b} = |\mathbf{a} \mathbf{b}|$. If [J] is singular, the five-bar mechanism is at an *output singularity*, indicating a workspace bound. In this case, there exist actuator velocities in the nullspace of [J] that instantaneously do not produce any end-effector velocity. The output singularities bound regions in the configuration space known as output modes [9]. For example, the five-bar in Fig. 1(a) has six output modes that are shown as shaded regions in the task space. The workspace boundaries are output singularities viewed in the workspace of the mechanism which can occur in two ways:

1. Links of A_0 CP dyad align: When the angle between the links A_0 C and CP is zero, the *inner workspace boundary* is obtained which is circular with radius R_I as seen in Fig. 1(a). Similarly, the circular *outer workspace boundary* with radius R_O is obtained when the angle between the links A_0 C and CP is π .

2. Links of $\mathbf{B}_0\mathbf{D}\mathbf{F}$ dyad align: Enforcing zero angle between $\mathbf{B}_0\mathbf{D}$ and $\mathbf{D}\mathbf{F}$ on two degree-of-freedom (DoF) five-bar leads to one DoF four-bar motion generating a coupler curve at \mathbf{P} which is the *folded workspace boundary* of the five-bar. Similarly, *extended workspace boundary* is obtained when the angle between $\mathbf{B}_0\mathbf{D}$ and $\mathbf{D}\mathbf{F}$ is π . These boundaries along with the four-bars are shown in Fig. 1(b).

The $\mathbf{B_0DF}$ dyad workspace boundaries are algebraic curves of degree higher than the $\mathbf{A_0CP}$ dyad workspace boundaries. Hence, the former can produce more customized shapes. This motivates shaping the extended and folded workspace boundaries of the five-bar mechanism and the procedure for the same is presented in the next section.

3 Problem Formulation

The problem of shaping the folded and extended workspace boundaries of the five-bar mechanism is formulated in this section. The extended and folded workspace boundaries of the five-bar mechanism are coupler curves of four-bar mechanisms $\mathbf{A}_0\mathbf{C}_e\mathbf{P}_e\mathbf{F}_e\mathbf{B}_0$ and $\mathbf{A}_0\mathbf{C}_f\mathbf{P}_f\mathbf{F}_f\mathbf{B}_0$, respectively, resulting from the alignment of the links in $\mathbf{B}_0\mathbf{D}\mathbf{F}$ dyad as explained in Sect. 2. These four-bars are shown in Fig. 1(b) where their joints are indexed¹ by i or j when their endeffectors are at \mathbf{P}_{e_i} or \mathbf{P}_{f_j} , respectively. Thus, the problem can be posed as synthesizing two four-bar with some shared dimensions whose coupler curves follow desired shapes. Note that the links $\mathbf{B}_0\mathbf{F}_e$ and $\mathbf{B}_0\mathbf{F}_f$ have different lengths while the rest of the dimensions are common between the two four-bars as seen in Fig. 1(b). The lengths of links $\mathbf{A}_0\mathbf{C}_e$ (or $\mathbf{A}_0\mathbf{C}_f$) and $\mathbf{C}_e\mathbf{P}_e$ (or $\mathbf{C}_f\mathbf{P}_f$) are denoted by r_{AC} and r_{CP} , respectively. The problem is formulated to first compute r_{AC} and r_{CP} which are common between the two four-bars and subsequently, compute the remaining dimensions of the four-bar mechanisms.

The desired shapes of the extended and folded workspace boundaries are specified by the points \mathbf{P}_{e_i} , $i=1,2,\ldots,n_{\rm e}$ and \mathbf{P}_{f_j} , $j=1,2,\ldots,n_{\rm f}$, respectively, that need to be followed as closely as possible. For this, the specified points must at least be reachable by $\mathbf{A}_0\mathbf{C}_{\rm e}\mathbf{P}_{\rm e}$ and $\mathbf{A}_0\mathbf{C}_{\rm f}\mathbf{P}_{\rm f}$ dyads:

$$R_I \le \|\mathbf{A}_0 - \mathbf{P}_{e_i}\| \le R_O, \quad R_I \le \|\mathbf{A}_0 - \mathbf{P}_{f_i}\| \le R_O.$$
 (4)

Let d_{\min} and d_{\max} denote the minimum and maximum distance between the specified points and \mathbf{A}_0 . Given the minimum allowable distance ϵ_O between the specified points and the outer workspace boundary, the radius $R_O = d_{\max} + \epsilon_O$. Similarly, $R_I = d_{\min} - \epsilon_I$ where ϵ_I is the minimum allowable distance between the specified points and the inner workspace boundary. Thus, r_{AC} and r_{CP} have two solutions:

 $^{^1}$ The indices are dropped to represent the joints for any general end-effector point $P_{\rm e}$ or $P_{\rm f}.$

$$r_{AC} = \frac{R_I + R_O}{2}, \quad r_{CP} = \frac{R_O - R_I}{2}, \quad \text{and}$$
 (5)

$$r_{AC} = \frac{R_O - R_I}{2}, \quad r_{CP} = \frac{R_I + R_O}{2}$$
 (6)

Recognizing that the four-bars for Eq. (5) are cognates of those for Eq. (6), the rest of the problem is solved considering only one of the solutions among Eqs. (5, 6).

Let the coordinates of \mathbf{B}_0 in $\{1\}$ be $\mathbf{B}_0 = [B_{x_0}, B_{y_0}]^{\top}$. The lengths of the links $\mathbf{B}_0\mathbf{F}_e$ and $\mathbf{B}_0\mathbf{F}_f$ are given by r_{BF_e} and r_{BF_f} , respectively. Having computed r_{CP} , the dimensions of $\mathbf{C}_e\mathbf{F}_e\mathbf{P}_e$ (or $\mathbf{C}_f\mathbf{F}_f\mathbf{P}_f$) link are fully determined by specifying the coordinates of \mathbf{F}_e (or \mathbf{F}_f) relative to \mathbf{C}_e (or \mathbf{C}_f). For this, a local frame $\{2\}$ is defined with its origin at \mathbf{C}_e (or \mathbf{C}_f) and x-axis along $\mathbf{C}_e\mathbf{P}_e$ (or $\mathbf{C}_f\mathbf{P}_f$) as shown in Fig. 1(b). The coordinates of \mathbf{F}_e and \mathbf{F}_f in $\{2\}$ are identical and are given by $\mathbf{f} = [f_x, f_y]^{\top}$. Therefore, the unknown variables in this problem are:

$$\mathbf{d}_{\text{fe}} = [f_x, f_y, B_{x_0}, B_{y_0}, r_{BF_e}, r_{BF_f}]^{\top}.$$
 (7)

With the end-effector \mathbf{P} at each \mathbf{P}_{e_i} , the coordinates of \mathbf{C}_{e_i} (see Fig. 1(b)) and the orientation of $\mathbf{C}_{e_i}\mathbf{P}_{e_i}$, denoted by β_{e_i} , are computed from the inverse kinematics (IK) of $\mathbf{A}_0\mathbf{C}_e\mathbf{P}_e$ dyad. For each \mathbf{P}_{e_i} , two IK solutions, i.e., "elbow-up" and "elbow-down" configurations, exist which belong to two different output modes of $\mathbf{A}_0\mathbf{C}_e\mathbf{P}_e$ dyad. In this manuscript, all the solutions $\mathbf{C}_{e_i}, \beta_{e_i}, i = 1, 2, \dots, n_e$ are found confining² to only one of the output modes of $\mathbf{A}_0\mathbf{C}_e\mathbf{P}_e$ dyad. The coordinates of \mathbf{F}_e in $\{1\}$ is:

$$\mathbf{F}_{e_i} = \mathbf{C}_{e_i} + [\mathcal{R}(\beta_{e_i})] \mathbf{f}. \tag{8}$$

Similarly, for all \mathbf{P}_{f_j} , the coordinates of \mathbf{C}_{f_j} , and the orientation of $\mathbf{C}_{f_j}\mathbf{P}_{f_j}$, i.e., β_{f_j} are found confining to only one of the output modes of $\mathbf{A}_0\mathbf{C}_f\mathbf{P}_f$ dyad. In this case, the location of \mathbf{F}_f in $\{1\}$ is found as:

$$\mathbf{F}_{\mathbf{f}_{i}} = \mathbf{C}_{\mathbf{f}_{i}} + \left[\mathcal{R}(\beta_{\mathbf{f}_{i}}) \right] \mathbf{f}. \tag{9}$$

Following the kinematic constraints of the four-bar mechanisms, the distances of \mathbf{F}_{e_i} and \mathbf{F}_{f_j} from \mathbf{B}_0 must be the link lengths r_{BF_e} and r_{BF_f} , respectively:

$$\|\mathbf{F}_{e_i} - \mathbf{B}_0\| = r_{BF_e}, \quad \|\mathbf{F}_{f_j} - \mathbf{B}_0\| = r_{BF_f}, \quad i = 1, 2, \dots, n_e, \quad j = 1, 2, \dots, n_f.$$
(10)

If $n_{\rm e} + n_{\rm f} \leq 6$, the constraints in Eq. (10) can be exactly satisfied by solving for $\mathbf{d}_{\rm fe}$. For $n_{\rm e} + n_{\rm f} = 6$, the number of constraints and variables are equal, and

² Subsets of IK solutions for $\mathbf{A}_0\mathbf{C}_e\mathbf{P}_e$ dyad can belong to different output modes. If the IK solutions for \mathbf{P}_{e_k} and $\mathbf{P}_{e_{k+1}}$ belong to different output modes, the portion of the extended workspace boundary between \mathbf{P}_{e_k} and $\mathbf{P}_{e_{k+1}}$ touches the inner or outer workspace boundary. Further study in this direction is considered for future work.

finitely many solutions are obtained. If $n_{\rm e} + n_{\rm f} < 6$, infinitely many solutions are obtained for ${\bf d}_{\rm fe}$. If $n_{\rm e} + n_{\rm f} > 6$, Eq. (10) becomes an over-constrained system which, in general, cannot be satisfied exactly. Hence, an optimization approach is adopted where the objective is to compute ${\bf d}_{\rm fe}$ such that the kinematic constraints in Eq. (10) are approximately satisfied with minimum residual. The residuals are given by:

$$r_{e_i} = (\|\mathbf{F}_{e_i} - \mathbf{B}_0\|^2 - r_{BF_e}^2)^2, \quad r_{f_j} = (\|\mathbf{F}_{f_j} - \mathbf{B}_0\|^2 - r_{BF_f}^2)^2.$$
 (11)

The objective is to minimize the total residual, denoted by r, given by:

$$\min_{\mathbf{d}_{fe}} r = \left(\sum_{i=1}^{n_e} r_{e_i}\right) + \left(\sum_{j=1}^{n_f} r_{f_j}\right). \tag{12}$$

In Eqs. (8, 9), \mathbf{F}_{e_i} , \mathbf{F}_{f_j} are obtained by choosing output modes for $\mathbf{A}_0\mathbf{C}_e\mathbf{P}_e$ and $\mathbf{A}_0\mathbf{C}_f\mathbf{P}_f$ dyads. Since two output modes are possible for each dyad, a total of $2^2 = 4$ sets of \mathbf{F}_{e_i} , \mathbf{F}_{f_j} are obtained which give rise to four objective functions, namely, r_k , k = 1, 2, 3, 4, according to Eq. (12). A solution method to solve the optimization problem for each r_k is presented in the next section.

4 Solution Method

All the objective functions r_k are polynomials of total degree four in \mathbf{d}_{fe} that differ only in terms of the coefficients of their monomials. Therefore, the number of critical points and the solution method are the same for all r_k . The critical points of r_k are obtained by setting the gradient $\frac{\partial r_k}{\partial \mathbf{d}_{\mathrm{fe}}} = \mathbf{0}$ and solving for \mathbf{d}_{fe} . This gives rise to six polynomial equations of total degree 324 in six variables \mathbf{d}_{fe} . Since the polynomial system does not contain all possible monomials in \mathbf{d}_{fe} , the number of finite solutions is expected to be less than the Bezout limit of 324. In fact, the number of finite solutions can be at most 81 found using parameter homotopy in Bertini [10].

Given the points $\mathbf{A}_0, \mathbf{P}_{e_i}, \mathbf{P}_{f_j}$ and the values for ϵ_O and ϵ_I , the critical points of r_k are computed by solving $\frac{\partial r_k}{\partial \mathbf{d}_{f_e}} = \mathbf{0}$ using Bertini. The critical points are saddles of index³ ranging from zero to six, where an index-0 saddle is a minimum and an index-6 saddle is a maximum. For any given $\mathbf{A}_0 = [A_{x_0}, A_{y_0}]^{\top}, \mathbf{P}_{e_i}, \mathbf{P}_{f_j}, \epsilon_O, \epsilon_I$, the solution $\mathbf{d}_{f_e}^* = [0 \ 0 \ A_{x_0} \ A_{y_0} \ r_{AC} \ r_{AC}]^{\top}$ (see Eqs. (5, 6) for r_{AC}) is a global minimum where the value of the objective function is $r_k^* = 0, \forall k = 1, 2, 3, 4$. For $\mathbf{d}_{f_e}^*$, the four-bars obtained are identical with \mathbf{A}_0 and \mathbf{C}_e (or \mathbf{C}_f) coinciding with \mathbf{B}_0 and \mathbf{F}_e (or \mathbf{F}_f), respectively. In this case, the four-bars are equivalent to a serial 2R chain defined by dyad $\mathbf{A}_0\mathbf{C}_e\mathbf{P}_e$ whose end-effector can reach every given point \mathbf{P}_{e_i} , \mathbf{P}_{f_j} while satisfying the kinematic constraints in Eq. (10) exactly giving $r_k^* = 0, \forall k = 1, 2, 3, 4$.

³ Index of a critical point is the number of principal directions of negative curvature, i.e. the number of negative eigenvalues of the Hessian matrix evaluated at the critical point.

Starting from each saddle point, gradient descent paths to minima are computed following [8]. These paths are represented as edges of a saddle graph whose nodes are the critical points. A point on a gradient descent path gives a point in the design space \mathbf{d}_{fe} , i.e., the dimensions of the four-bar mechanisms $\mathbf{A}_0\mathbf{C}_e\mathbf{P}_e\mathbf{F}_e\mathbf{B}_0$ and $\mathbf{A}_0\mathbf{C}_f\mathbf{P}_f\mathbf{F}_f\mathbf{B}_0$. The corresponding five-bar mechanism has the dimensions of the links $\mathbf{A}_0\mathbf{C}$ and \mathbf{CPF} same as $\mathbf{A}_0\mathbf{C}_e$ (or $\mathbf{A}_0\mathbf{C}_f$) and $\mathbf{C}_e\mathbf{P}_e\mathbf{F}_e$ (or $\mathbf{C}_f\mathbf{P}_f\mathbf{F}_f$), respectively. The lengths of links $\mathbf{B}_0\mathbf{D}$ and \mathbf{DF} are $r_{BD}=(r_{BF_e}+r_{BF_f})/2$ and $r_{DF}=(r_{BF_e}-r_{BF_f})/2$, respectively. Swapping the links $\mathbf{B}_0\mathbf{D}$ and \mathbf{DF} results in a different five-bar mechanism that has the same workspace boundaries. Additionally, from the cognates of the fourbars $\mathbf{A}_0\mathbf{C}_e\mathbf{P}_e\mathbf{F}_e\mathbf{B}_0$ and $\mathbf{A}_0\mathbf{C}_f\mathbf{P}_f\mathbf{F}_f\mathbf{B}_0$, two more five-bar mechanisms can be obtained. Therefore, for a solution of \mathbf{d}_{fe} , four five-bar mechanism with the desired workspace boundary in the next section.

5 Numerical Example

In this section, a numerical example is presented where the goal is to synthesize a five-bar mechanism that has "flat" velocity ellipses with minor axes oriented almost vertically throughout the bottom portion of its workspace. To achieve this, the extended workspace boundary is desired to be nearly horizontal by closely following the line $L_{\rm e}$ given by:

$$L_{\rm e}: \mathbf{p}_{\rm e}(\alpha_{\rm e}) = \alpha_{\rm e}[-0.112 \ -0.049]^{\top} + (1 - \alpha_{\rm e})[-0.159 \ -0.025]^{\top}.$$
 (13)

For a larger portion of the workspace to have "flat" ellipses, the folded workspace boundary is also desired to be as horizontal as possible. By trial and error, desirable results were obtained if the folded workspace boundary closely followed the line $L_{\rm f}$ given by:

$$L_{\rm f}: \mathbf{p}_{\rm f}(\alpha_{\rm f}) = \alpha_{\rm f}[-0.097 \ -0.095]^{\top} + (1 - \alpha_{\rm f})[-0.149 \ -0.092]^{\top}.$$
 (14)

The lines $L_{\rm e}$ and $L_{\rm f}$ are chosen to lie below the ground pivot $\mathbf{A}_0 = \begin{bmatrix} 0 & 0 \end{bmatrix}^{\mathsf{T}}$ so that the region between them can be the portion of the workspace where "flat" velocity ellipses may be possible. Further, ground pivot \mathbf{B}_0 is desired to lie above $L_{\rm e}$, $L_{\rm f}$ to maintain a location suitable for applications.

From $L_{\rm e}$, $n_{\rm e}=100$ points are uniformly sampled to get ${\bf P}_{\rm e_i}$. Similarly, $n_{\rm f}=100$ points are sampled from $L_{\rm f}$ to get ${\bf P}_{\rm f_j}$. Further, $\epsilon_O=0.004, \epsilon_I=0.04$ were chosen. The link lengths r_{AC}, r_{CP} are found using Eq. (6). Following Sect. 4, the optimization problem was solved for each $r_k, k=1,2,3,4$ using Bertini. The magnitude of perturbation $h=10^{-4}$ to compute the gradient descent paths in the saddle graph. Choosing "elbow-up" configurations for both ${\bf A}_0{\bf C}_{\rm e}{\bf P}_{\rm e}$ and ${\bf A}_0{\bf C}_{\rm f}{\bf P}_{\rm f}$ dyads to find ${\bf F}_{\rm e_i}, {\bf F}_{\rm f_j}$ in Eqs. (8, 9), the solutions obtained are shown in Fig. 2. All the saddle points are seen to connect to the global minimum along gradient descent paths. Although the saddle solutions in Figs. 2(b)-2(d) that follow $L_{\rm e}, L_{\rm f}$ closely, they are not desirable since the workspace is not entirely the

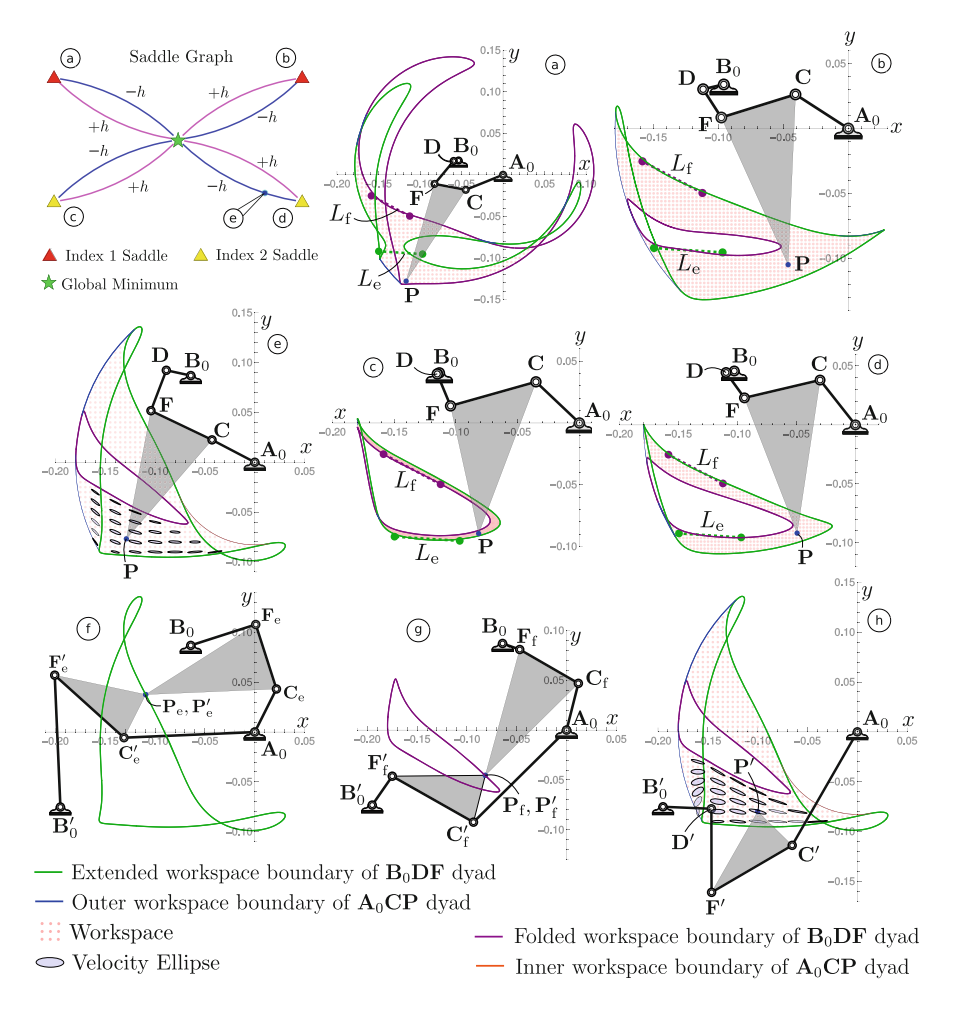


Fig. 2. Saddle graph and solutions for five-bar whose portions of extended and folded workspace boundaries closely follow $L_{\rm e}$ and $L_{\rm f}$ in Eqs. (13, 14), respectively. In the saddle graph, edges labelled +h and -h correspond to gradient descent paths obtained by perturbing the saddle point along positive and negative eigenvector, respectively, along the steepest descent direction.

regions between $L_{\rm e}$, $L_{\rm f}$. In cases like Fig. 2(c), the workspace can also be very narrow due to small ${\bf B}_0 {\bf D}$ link length. However, exploring designs along the gradient descent paths, the solution in Fig. 2(e) is a possible candidate that meets all the criteria mentioned previously in this section. Interchanging the links of ${\bf A}_0 {\bf CP}$ dyad gives another five-bar that has the same workspace boundaries.

The cognates of $\mathbf{A}_0\mathbf{C}_e\mathbf{P}_e\mathbf{F}_e\mathbf{B}_0$ and $\mathbf{A}_0\mathbf{C}_f\mathbf{P}_f\mathbf{F}_f\mathbf{B}_0$ are $\mathbf{A}_0\mathbf{C}_e'\mathbf{P}_e'\mathbf{F}_e'\mathbf{B}_0'$ and $\mathbf{A}_0\mathbf{C}_f'\mathbf{P}_f'\mathbf{F}_f'\mathbf{B}_0'$ as shown in Figs. 2(f) and 2(g), respectively (formulas given in [11, Eq. (16)]). These four-bars can be used to find another five-bar mechanism

in Fig. 2(h) that has the same workspace boundaries as in Fig. 2(e). Finally, the fourth five-bar that has the same workspace boundary is found by swapping the links of $\mathbf{A}_0'\mathbf{C}'\mathbf{P}'$ dyad.

From Fig. 2(e) it can be seen that the majority of the velocity ellipses in the bottom workspace are nearly "flat". This has been achieved by shaping portions of the extended and folded workspace boundaries as roughly horizontal straight lines.

6 Conclusion

The concept of shaping workspace boundaries to tune the first-order kinematics of a mechanism was proposed in this work. A five-bar mechanism was considered to demonstrate this concept. Given one of the ground pivots and the desired shape of the workspace boundary, a method to synthesize five-bar mechanisms was presented. The method was used to synthesize a five-bar mechanism with portions of its workspace boundaries being roughly horizontal. By achieving this shape of the workspace boundaries, it was shown that the minor axes of the velocity ellipses could be oriented almost vertically in the region between the shaped workspace boundaries.

Acknowledgement. This material is based upon work supported by the National Science Foundation under Grant No. CMMI-2144732.

References

- Starns, G., Flugrad, D.R., Jr.: Five-bar path generation synthesis by continuation methods. J. Mech. Des. 115(4), 988-994 (1993). https://doi.org/10.1115/1.2919297
- Buśkiewicz, J.: Use of shape invariants in optimal synthesis of geared five-bar linkage. Mech. Mach. Theory 45(2), 273–290 (2010). https://doi.org/10.1016/j. mechmachtheory.2009.09.004
- Koutsoukis, K., Papadopoulos, E.: On the effect of robotic leg design on energy efficiency. In: IEEE International Conference on Robotics and Automation (ICRA), vol. 2021, pp. 9905–9911 (2021). https://doi.org/10.1109/ICRA48506. 2021.9560997
- Duc Sang, N., Matsuura, D., Sugahara, Y., Takeda, Y.: Kinematic design of five-bar parallel robot by kinematically defined performance index for energy consumption.
 In: Corves, B., Wenger, P., Hüsing, M. (eds.) EuCoMeS 2018. MMS, vol. 59, pp. 239–247. Springer, Cham (2019). https://doi.org/10.1007/978-3-319-98020-1_28
- Demjen, T., Lovasz, E.-C., Ceccarelli, M., Sticlaru, C., Lupuţi, A.-M.-F., Oarcea, A., Silaghi-Perju, D.-C.: Design of the five-bar linkage with singularityfree workspace. Robotica 41(11), 3361–3379 (2023). https://doi.org/10.1017/ S0263574723001042
- Liu, X.-J., Wang, J., Pritschow, G.: Performance atlases and optimum design of planar 5R symmetrical parallel mechanisms. Mech. Mach. Theory 41(2), 119–144 (2006). https://doi.org/10.1016/j.mechmachtheory.2005.05.003

- Plecnik, M.: Ellipse synthesis of a five-bar linkage. In: 46th Mechanisms and Robotics Conference (MR), International Design Engineering Technical Conferences and Computers and Information in Engineering Conference, vol. 7, p. V007T07A081 (2022). https://doi.org/10.1115/DETC2022-91341.
- Baskar, A., Plecnik, M., Hauenstein, J.D.: Computing saddle graphs via homotopy continuation for the approximate synthesis of mechanisms. Mech. Mach. Theory 176, 104932 (2022). https://doi.org/10.1016/j.mechmachtheory.2022.104932
- Edwards, P.B., Baskar, A., Hills, C., Plecnik, M., Hauenstein, J.D.: Output mode switching for parallel five-bar manipulators using a graph-based path planner. In. IEEE International Conference on Robotics and Automation (ICRA), vol. 2023, pp. 9735–9741 (2023). https://doi.org/10.1109/ICRA48891.2023.10160891
- 10. Bates, D.J., Hauenstein, J.D., Sommese, A.J., Wampler, C.W.: Bertini: software for numerical algebraic geometry https://doi.org/10.7274/R0H41PB5, https://doi.org/10.7274/
- Plecnik, M.M., Fearing, R.S.: A study on finding finite roots for kinematic synthesis. In: ASME 2017 International Design Engineering Technical Conferences and Computers and Information in Engineering Conference, American Society of Mechanical Engineers, pp. V05BT08A083-V05BT08A083 (2017). https://doi.org/10.1115/DETC2017-68341